ON-AXIS TREATMENT METHOD OF THE BOR-FDTD ALGORITHM AND ITS APPLICATIONS

Miaomiao LI[1,*], Jie JI[2], Shanshan SHEN[3]

Originating from the standard Finite-Difference Time-Domain (FDTD) method, the Body of Revolution FDTD (BOR-FDTD) algorithm stands out as a high-efficiency computational paradigm, dedicated to simulating the propagation behaviors of electromagnetic waves in structures with pure symmetry, e.g., fiber optic cables and antenna configurations While BOR-FDTD leverages axisymmetric properties to avoid azimuthal discretization—thereby improving computational efficiency—the mathematical singularity of electro-magnetic field components on the axis requires special attention. To address the loss of accuracy caused by inadequate treatment of on-axis field components in BOR-FDTD, this study first analyzes the field quantities requiring special treatment based on the discretized equations of the algorithm. Subsequently, Stokes' theorem is applied in conjunction with periodic boundary conditions, and azimuthal field values are integrated to derive final expressions for these on-axis field components. Finally, the proposed treatment method is implemented in three simulation scenarios: scatterers with Mur absorbing boundaries, perfectly matched layer (PML) absorbers, and fiber optic cable resonant cavities. Results demonstrate that the on-axis treatment significantly enhances computational accuracy without compromising efficiency or memory usage.

Keywords: The body of revolution, Finite-difference time-domain algorithm, Special treatment on-axis, Stokes' theorem, Periodic boundary conditions

1. Introduction

The Finite-Difference Time-Domain (FDTD) algorithm, a computational electromagnetics numerical scheme proposed by K.S. Yee in 1996, was developed specifically to achieve efficient solutions for the fundamental Maxwell equations of electromagnetic fields [1,2]. This method is suitable for multi-threaded parallel computing and features high accuracy, strong systematicness, space-saving storage, and strong universality [3]. It is well-suited for simulating various complex structures and is widely used in analyzing various electromagnetic phenomena, such as EMR analysis [4], radio wave propagation, electromagnetic coupling, nuclear explosion and lightning pulse propagation, etc. [5-7]. Compared with the

[1]* MSc., School of Electronic Information Engineering/School of Integrated Circuits, Nanjing University of Industry Technology, Nanjing, 210023, China, corresponding author: e-mail: pzlimiaomiao@163.com.
[2] MSc., School of Transportation Economics and Management, Nanjing Vocational Institute of Railway Technology, Nanjing, 210031, China, e-mail: jannedarc@live.cn.
[3] Prof., School of Electronic Information Engineering/School of Integrated Circuits, Nanjing University of Industry Technology, Nanjing, 210023, China, e-mail: ssssoner@163.com.

Method of Moments (MoM) [8], the Finite Element Method (FEM) [9], and high-frequency approximation methods, the advantage of the FDTD algorithm lies in that it can obtain all electromagnetic field information through a single time-domain solution According to the solution principle of the FDTD algorithm, its central difference process involves performing finite difference discretization on electric/magnetic field quantities in both time and space. It uses a series of discrete values to represent the continuous values of each variable in the electromagnetic field [10], thereby realizing the propagation of electromagnetic field waveforms in the time domain. Alternatively, it can be understood that the electric/magnetic field value at each grid point depends on the magnetic/electric field values at the surrounding half-grid points [11]. Unlike the Cartesian coordinate system, the cylindrical FDTD algorithm performs finite difference discretization and solution in space along the radial ρ, angular ϕ, and axial z directions respectively. In fact, its $\rho o \phi$ plane is a periodic cyclic structure formed by the superposition of sectors corresponding to different ϕ values. According to the description of the BOR-FDTD algorithm [12-14], its core lies in utilizing axial symmetry and realizing the transformation from the FDTD algorithm in the 3D cylindrical coordinate system to BOR-FDTD through the concept of periodic cycling. In addition, since electric/magnetic field quantities also exist on the z-axis, when $\rho = 0$, the electric/magnetic field quantities on the axis exhibit mathematical singularity. Meanwhile, due to the presence of the $1/\rho$ term in some electric/magnetic field equations of the FDTD algorithm, the calculation of electric/magnetic field quantities on the z-axis will be lost in the process of avoiding the $1/\rho$ term by using the selection of the ρ-direction range. Therefore, the FDTD algorithm needs a special treatment for the electric/magnetic field of z-axis in the cylinder. Obviously, the BOR-FDTD algorithm derived from the FDTD algorithm cannot ignore the special treatment of the z-axis electric/magnetic field quantities; otherwise, the lack of calculation of the electromagnetic field quantities on the axis will also affect its calculation accuracy under the application model.

To investigate the special handling issue of the on-axis (z-axis) quantities in the BOR-FDTD algorithm, the main innovations and research contents of this paper are as follows:

(1) Expand the finite difference discretization equations of the BOR-FDTD algorithm, judge the finite difference discretization equations of all electric/magnetic field quantities one by one through the position variation of radial grid points, and then obtain the final electric/magnetic field quantities that require special on-axis (z-axis) handling.

(2) Use Stokes' theorem to derive the BOR-FDTD time-domain equations for the electric/magnetic field quantities that need special on-axis (z-axis) handling.

(3) Through three numerical simulation examples, verify the impact of the proposed on-axis special handling method on the calculation error and efficiency of the BOR-FDTD algorithm.

2. Theoretical Elaboration and Analysis of the Method

2.1 Analysis of Obtaining Special-Processed Field Quantities on the Axis

2.1.1 Analysis of On-Axis Processing in Three-Dimensional Cylindrical Coordinate FDTD Algorithm

Combined with the concept of periodic cycling, the spatial distribution of the Yee cell for electric/magnetic field quantities in the 3D cylindrical coordinate FDTD algorithm is shown in the left part of Fig. 1 [15]. Obviously, the unit cross-section ($\rho o\phi$ plane) is a partial circular ring, and the Yee cell spatial distribution of electric/magnetic fields in the 3D cylindrical coordinate FDTD algorithm can be formed by accumulating multiple such $\rho o\phi$ cross-sections around the z-axis. Thus, when the $\rho o\phi$ cross-section is infinitely small, the special solution for the z-axis in the 3D cylindrical coordinate FDTD algorithm can be positioned as solving the electric/magnetic field quantities of the $\rho o\phi$ cross-section; that is, according to the FDTD spatial difference principle, each electric/magnetic field quantity on the z-axis can be solved using the electric/magnetic fields of the $\rho o\phi$ cross-section. As shown on the right side of Fig. 1, in the calculation of electric/magnetic field quantities of the $\rho o\phi$ cross-section, the unit cross-section adjacent to the z-axis can degenerate from a partial circular ring into a sector. Furthermore, by accumulating multiple such sectors (where the variation of sector positions in the ϕ-direction follows $j_1 = 1, 2, ..., j_{\max}$), the finite difference discrete units of each field quantity under the 3D cylinder can be formed. By comparing the left and right parts of Fig. 1, it can be seen that all electric/magnetic field quantities exhibit mathematical singularity on the axis where $\rho = 0$. Specifically, due to the variation of the vector direction of the field quantities (e_ϕ and h_ρ) with ϕ, their positions at the discrete units adjacent to the z-axis are meaningless and will disappear naturally. Furthermore, it can be concluded that when the half-grid point $d = 1/2$, the only electric/magnetic field quantities requiring special handling for their discrete unit positions are $e_z(0, j, k+1/2)$ and $h_z(1/2, j+1/2, k)$.

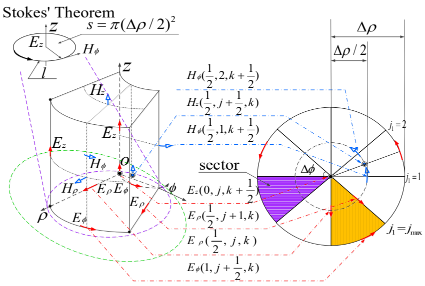

Fig. 1. Analysis of special treatment on the z-axis in 3D cylindrical coordinate system

2.1.2 Analysis of On-Axis Processing in the BOR-FDTD Algorithm

As shown in Fig. 2, the BOR-FDTD algorithm leverages the axial symmetry of 3D purely symmetric cylinders to map the 3D spatial Yee cells of the FDTD algorithm onto the ρoz plane [16,17]. It then forms a purely symmetric cylindrical structure by rotating around the z-axis with different azimuthal modes m. Furthermore, the computational efficiency of the FDTD algorithm for 3D purely symmetric cylinders is improved through the accumulation of a limited number of modes. Obviously, in the BOR (Body of Revolution), the FDTD algorithm does not need to consider the finite difference discretization of electric/magnetic field quantities in the ϕ-direction.

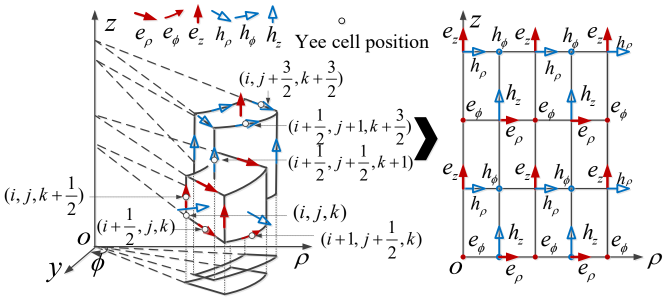

Fig. 2. Mapping of FDTD algorithm from 3D to 2D

Here, the matrix representation and coefficient matrix $\boldsymbol{R}$ of the BOR-FDTD algorithm from reference [18] are directly given as follows:

$$\left(\left(\boldsymbol{W}^{n+1}-\boldsymbol{W}^{n}\right)/\Delta t\right)=\boldsymbol{R}\boldsymbol{W}, \tag{1}$$

$$\boldsymbol{R}=\begin{bmatrix} 0 & \boldsymbol{R}_1/\mu_0 \\ \boldsymbol{R}_2/\varepsilon_0 & 0 \end{bmatrix}_{6\times 6}, \tag{2}$$

$$\boldsymbol{R}_1=\begin{bmatrix} 0 & \partial z & \pm m/\rho \\ -\partial z & 0 & \partial\rho \\ \mp m/\rho & -(1/\rho)(\partial\rho)\rho & 0 \end{bmatrix}_{3\times 3}, \tag{3}$$

$$\boldsymbol{R}_2=\begin{bmatrix} 0 & -\partial z & \pm m/\rho \\ \partial z & 0 & -\partial\rho \\ \mp m/\rho & (1/\rho)(\partial\rho)\rho & 0 \end{bmatrix}_{3\times 3}, \tag{4}$$

Among them, n denotes the time step, $\partial_i(i=\rho,z)$ represents the first-order finite difference discretization along the ρ-(radial) and z-(axial) directions in the BOR-FDTD algorithm, m is the azimuthal mode number, ε_0 and μ_0 stand for electrical conductivity and magnetic permeability, respectively.

Evidently, according to the principle of the BOR-FDTD algorithm, the field quantities requiring special treatment on the z-axis at this time are $e_z(0,k+1/2)$ and $h_z(1/2,k)$. To further verify the existence of the electric and magnetic field quantities that require special on-axis (z-axis) treatment in the BOR-FDTD algorithm, this section performs spatial finite difference discretization and expansion on the basic equations of BOR-FDTD. By examining the variation of field quantities across all grid points from $\rho=0$ to $\rho_{\max}$, each electric and magnetic field quantity is evaluated individually to identify the final set of quantities that need special on-axis processing. After conducting a simplified temporal and spatial finite difference discretization expansion (following the FDTD algorithm) on each electric and magnetic field quantity in Equation 3-(30) of Reference [19], the results are obtained as follows:

$$\begin{aligned}&h_\rho^{n+1/2}(i,k+1/2)-h_\rho^{n-1/2}(i,k+1/2)=\\&\frac{\Delta t}{\mu}\Big[\big(e_\phi^n(i,k+1)-e_\phi^n(i,k)\big)/\Delta z\pm me_z^n(i,k+1/2)/\big(i\Delta\rho\big)\Big],\end{aligned}\tag{5}$$

$$\begin{aligned}&h_\phi^{n+1/2}(i+1/2,k+1/2)-h_\phi^{n-1/2}(i+1/2,k+1/2)=\\&\frac{\Delta t}{\mu\Delta\rho}\begin{bmatrix}e_z^n(i+1,k+1/2)\\-e_z^n(i,k+1/2)\end{bmatrix}-\frac{\Delta t}{\mu\Delta z}\begin{bmatrix}e_\rho^n(i+1/2,k+1)\\-e_\rho^n(i+1/2,k)\end{bmatrix},\end{aligned}\tag{6}$$

$$\begin{aligned}&h_z^{n+1/2}(i+1/2,k)-h_z^{n-1/2}(i+1/2,k)=\\&\frac{\Delta t}{\mu(i+1/2)\Delta\rho}\Big[\mp me_\rho^n(i+1/2,k)-(i+1)e_\phi^n(i+1,k)+ie_\phi^n(i,k)\Big],\end{aligned}\tag{7}$$

$$\begin{aligned}&e_\rho^{n+1}(i+1/2,k)-e_\rho^n(i+1/2,k)=\pm\frac{m\Delta t}{\varepsilon(i+1/2)\Delta\rho}h_z^{n+1/2}(i+1/2,k)\\&-\frac{\Delta t}{\varepsilon\Delta z}\Big[h_\phi^{n+1/2}(i+1/2,k+1/2)-h_\phi^{n+1/2}(i+1/2,k-1/2)\Big]\end{aligned},\tag{8}$$

$$\begin{aligned}&e_\phi^{n+1}(i,k)-e_\phi^n(i,k)=\frac{\Delta t}{\varepsilon\Delta z}\Big[h_\rho^{n+1/2}(i,k+1/2)-h_\rho^{n+1/2}(i,k-1/2)\Big]\\&-\frac{\Delta t}{\varepsilon\Delta\rho}\Big[h_z^{n+1/2}(i+1/2,k)-h_z^{n+1/2}(i-1/2,k)\Big]\end{aligned},\tag{9}$$

$$\begin{aligned}&e_z^{n+1}(i,k+1/2)-e_z^{n}(i,k+1/2)=\mp\frac{m\Delta t}{\varepsilon i\Delta\rho}h_\rho^{n+1/2}(i,k+1/2)\\&+\frac{\Delta t}{\varepsilon i\Delta\rho}\Big[(i+1/2)h_\phi^{n+1/2}(i+1/2,k+1/2)-(i-1/2)h_\phi^{n+1/2}(i-1/2,k+1/2)\Big]\end{aligned}, \quad (10)$$

Among them, i and k denote the spatial positions in the radial ρ and axial z directions in the BOR-FDTD algorithm, respectively.

Evidently, in the process of variation across all grid points from $\rho=0$ to $\rho_{\max}$, the h_ρ in Equation (5) and e_z in Equation (10) are the ones containing the $1/\rho$ term. However, the previous conclusion regarding the 3D cylindrical coordinate system has already indicated that e_ϕ and h_ρ do not require consideration during the z-axis processing. In the analysis here, it can be seen from the right-hand side of Equation (7) that since $\rho=0$ does not cause a solution overflow, $ie_\phi^n(i,k)$ renders e_ϕ meaningless in terms of solution. However, for h_ρ in Equation (5), during the spatial variation across all grid points along the ρ-direction, if $\rho=0$, it will cause an overflow in the discrete solution. By referring to Fig. 1 and 2 again here, it can be further illustrated that h_ρ in Equation (5) also does not require z-axis processing (since the solution of h_ρ requires the use of e_ϕ). Following the previous conclusion, for the field quantities requiring special on-axis (z-axis) treatment, namely e_z and h_z, when $\rho=0$, the first spatial position of h_z in Equation (7) along the ρ-direction is also $1/2$. This indicates that during the special on-axis processing, the special solution equation for $h_z(1/2,k)$ can follow the spatial variation from $\rho=0$ to $\rho_{\max}$, without the need to separately derive the solution for $\rho=0$. However, for e_z in Equation (10), when $\rho=0$, the denominator of the $1/\rho$ term tends to infinity, which causes an overflow in the solution. Therefore, a separate solution for $\rho=0$ must be derived. As for whether $h_z(1/2,k)$ (adjacent to the z-axis) requires a separate solution, further analysis is still needed.

Since the spatial variation of full grid points along the ρ-direction is a factor that affects whether the BOR-FDTD finite difference discrete solution overflows during the special on-axis (z-axis) processing, it is not advisable to arbitrarily set the full grid points along the ρ-direction to zero for solution calculation to avoid such overflow. Instead, starting from the physical meanings of $e_z(0,k+1/2)$ and $h_z(1/2,k)$, Stokes' theorem is applied to further perform the transformation of these two quantities from the frequency domain to the time domain.

As shown in Fig. 1, according to the curl theory, it can be known that the surface integral expansion of $e_z(0, j, k+1/2)$ in the frequency domain under the 3D cylindrical coordinate system is expressed as:

$$j\omega\varepsilon\int_s e_z ds = \int_s \hat{z}\cdot\left[\nabla\times\vec{h}\right]ds, \tag{11}$$

Among them, ∇ is the curl operator, $\vec{h}$ is the curl of the magnetic field vector, and the surface integral region is the s-plane shown in Fig. 1.

Therefore, according to Stokes' theorem [20], Equation (11) can be written as:

$$j\omega\varepsilon \int_s e_z\, ds = \oint_l \vec{h}\cdot d\vec{l}, \tag{12}$$

Among them, the path of the line integral is the boundary integral of the s-plane, and the direction of $d\overset{\vee}{l}$ and $\hat{z}$ satisfy the right-hand rule.

Converting Equation (12) to the time domain, we can obtain:

$$\varepsilon \int_s (\partial e_z/\partial t)\, ds = \oint_l \vec{h}\cdot d\vec{l}, \tag{13}$$

When the surface integral region has a radius of $\Delta\rho/2$ as shown in Fig. 1, the time-domain equation of $e_z(0, j, k+1/2)$ can be written as:

$$\begin{gathered}\pi\left(\Delta\rho/2\right)^2\varepsilon\left(\partial e_z(0,j,k+1/2)/\partial t\right) = \\ 2\pi\sum_{j_1=0}^{j_{\max}-1} h_\phi(1/2, j_1, k+1/2)\left(\Delta\rho/2\right)\Delta\phi\end{gathered}, \tag{14}$$

It is obvious that for the BOR-FDTD algorithm, $h_\phi(1/2, j_1, k+1/2)$ corresponding to $j_1 = 1, 2, \ldots\ldots, j_{\max}$ in different ϕ-directions are the same. Thus, Equation (14) can be transformed into the time-domain equation for $e_z(0, k+1/2)$ in the special on-axis (z-axis) processing of the BOR-FDTD algorithm as follows:

$$\partial e_z(0, k+1/2)/t = \left(4/\varepsilon\Delta\rho\right)h_\phi^{n+1/2}(1/2, k+1/2), \tag{15}$$

By the same reasoning as in the derivation of Equation (13), $h_z(1/2, k)$ can be expressed in the integral form of the magnetic field in the time domain along the z-direction as:

$$\mu \int_s (\partial h_z/\partial t)\, ds = -\oint_l \vec{e}\, d\vec{l}, \tag{16}$$

Recalling Fig. 1, in the 3D cylindrical coordinate system, when the radius is $\Delta\rho$, the time-domain equation of $h_z(1/2, j+1/2, k)$ can be written as:

$$\begin{gathered}\left(\mu\pi\Delta\rho^2\Delta\phi/2\pi\right)\left(\partial h_z(1/2, j+1/2, k)\right) = \\ -e_\phi(1, j+1/2, k)\Delta\rho\Delta\phi + \left[e_\rho(1/2, j+1, k) - e_\rho(1/2, j, k)\right]/\Delta\rho\end{gathered}, \tag{17}$$

Since the BOR-FDTD algorithm does not require considering the finite difference discrete transformation in the ϕ-direction, Equation (17) can be transformed into the time-domain equation of $h_z(1/2, k)$ for the special on-axis (z-

axis) processing in the BOR-FDTD algorithm. In this process, the e_ρ terms on the right-hand side of Equation (17) will cancel each other out, and e_ϕ does not need to be considered. In summary, during the special on-axis (z-axis) processing of the BOR-FDTD algorithm, $h_z(1/2,k)$ requires no special treatment, and only $e_z(0,k+1/2)$ needs to be handled.

3. Numerical Examples

To verify the necessity of axial (z-axis) processing in the BOR-FDTD algorithm, three numerical examples are provided here for validation, including the scatterer with Mur and perfectly matched layer (PML), and the fiber optic cable resonant cavity [21-23].

Example 1: Four-slot Scattering Model with Mur Absorbing Boundary Truncation

In free space, consider the four-slot perfect electric conductor (PEC) scatterer truncated by Mur absorbing boundaries as shown in Fig. 3. The scatterer has a radius of 21 cm and a height of 40 cm, with four uniformly distributed grooves on its outer side, each with a depth of 1 cm and a width of 2 cm. The grid sizes are $\Delta\rho$=Δz=1cm. An obliquely incident wave with $\theta_i = 45^o$ impinges on the Huygens surfaces at $\rho = 21.5$ cm and $z = \pm 21.5$ cm, and the incident electric field signal is:

$$E = E_0 \cos(2\pi f_0) \exp\left(-4\pi(t-t_0)/\tau\right)^2, \tag{18}$$

Where $E_0 = 1000$ V/m, $f_0 = 10$GHz, $\tau = 1.0/f_0$, $t_0 = 1.25/f_0$.

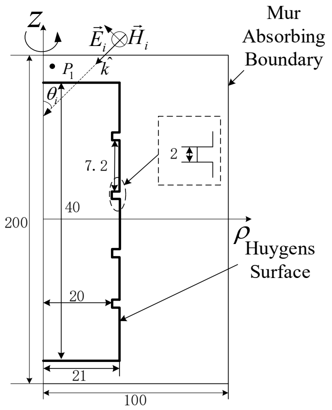

Fig. 3. Four-groove perfect electric conductor (PEC) scatterer

In this numerical example, the scatterer shown in Fig. 3 is truncated by a first-order Mur absorbing boundary with a size of 60cm×120cm around it. Meanwhile, an axial observation point is set as P_1 ($1\Delta\rho$, $50\Delta z$). Obviously, it can be seen from the simulation results in Fig. 4 that under this example, the BOR-FDTD algorithm with z-axis special processing agrees well with the reference values from

CST (a commercial simulation software) at the observation point P_1, while the algorithm without *z*-axis processing exhibits relatively significant errors.

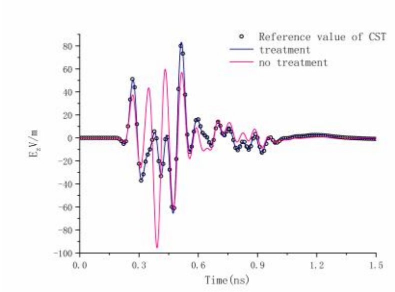

Fig. 4. The electric field waveforms at observation point P_1 in Example 1

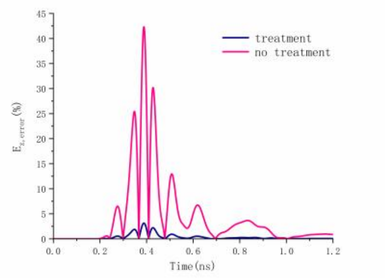

Fig. 5. Errors at observation point P_1 in Example 1

To further illustrate the application of the proposed z-axis special processing in improving the accuracy of the BOR-FDTD algorithm, the general error calculation formula is utilized here:

$$\text{error}_{\%} = \left| \left(E - E_{ref} \right) / E_{ref-\max} \right|, \tag{19}$$

Where E denotes the electric field values at observation point P_1 obtained with and without *z*-axis special processing, E_{ref} represents the reference value from CST (owing to the built-in adaptive and automatic mesh optimization technology of CST, a commercial electromagnetic simulation software, its electromagnetic simulation results are highly consistent with measured data, and thus the CST simulation data are usually used as reference values to verify the accuracy of the proposed algorithm), and $E_{ref-\max}$ is the maximum value of E_{ref} .

As shown in Fig. 5, by virtue of the high consistency between the CST simulation data and the measured data, combined with Equation (19), we can obtain the following results: the simulation results of Example 1 with and without *z*-axis special processing exhibit different error results at observation point P_1. The error with *z*-axis special processing is less than 5%, while the error without *z*-axis processing reaches about 43%, which can again illustrate the impact of the *z*-axis special processing scheme proposed in this paper on the accuracy of the BOR-FDTD algorithm.

Example 2: Single-Slot Scattering Model Truncated by PML Absorbing Boundaries

In free space, consider the single-slot perfect electric conductor (PEC) scatterer truncated by PML absorbing boundaries as shown in Fig. 6. The scatterer's radius, height, radial and axial grid sizes, as well as the oblique incident wave conditions and electric field signal, are consistent with those in Example 1. The differences lie in two aspects: first, a single groove with a depth of 4 cm and a height of 0.8 cm is cut at the center of the scatterer's outer side; second, the extended grid technique [24] is adopted to solve the electromagnetic field quantities inside this groove.

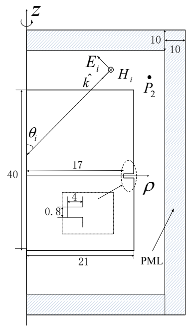

Fig. 6. Single-groove perfect electric conductor (PEC) scatterer

In this numerical example, the scatterer shown in Fig. 6 is truncated by a 10-layer (10cm thick) PML absorbing boundary at the 60cm×120cm boundary surrounding it. Meanwhile, in the simulation with PML boundary truncation, the electromagnetic field variation at the corner points is relatively intense. To make the example verification more convincing, an angular observation point is set as $P_2(50\Delta\rho, 50\Delta z)$ in this example. Obviously, similar to the conclusion of Example 1, the simulation results shown in Fig. 7 indicate that under this example, the BOR-FDTD algorithm with *z*-axis special processing still agrees well with the CST reference values at the observation point P_2. In contrast, the algorithm without *z*-axis processing cannot effectively absorb electromagnetic wave reflections due to the lack of calculation for the PML absorbing boundary along the axis, resulting in more significant errors.

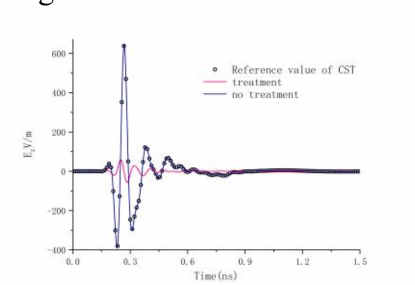

Fig. 7. The electric field waveforms at observation point P_2 in Example 2

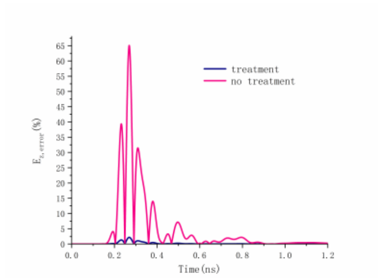

Fig. 8. Errors at observation point P_2 in Example 2

Similar to Example 1 (continuing to leverage the high consistency between CST simulation data and measured data), Equation (19) is still used here as the error calculation formula to compute the electric field error at observation point P_2. The error calculation results shown in Fig. 8 indicate that the error with *z*-axis special processing is still less than 5%, while the error without *z*-axis processing reaches approximately 65%. This can also further illustrate the impact of the proposed *z*-

axis special processing method in this paper on the calculation accuracy of the BOR-FDTD algorithm.

Example 3: Fiber Optic Cable Resonant Cavity

As shown in Fig. 9, this numerical example involves a purely symmetric coaxial cable cylinder with a radius of 1cm (317$\Delta\rho$) and a height of 2cm (634Δz), where $\Delta\rho$=Δz=0.003153cm and $\Delta\phi$ = 2π/40. Meanwhile, the incident wave from Equations (18) in Examples 1–2 is still used, incident at point S (0, 0) with an incident frequency of f0 = 4GHz. Observation points are set as P_3 (8,2), P_4 (10,6), P_5 (8, -2), and P_6 (10, -2), and the simulation results of the TM01 mode at points P_3–P_6 are calculated.

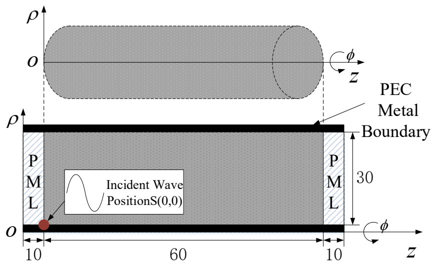

Fig. 9. Purely symmetric coaxial fiber optic cable cylindrical resonant cavity

Obviously, as shown in Fig. 10(a)–(d), after z-axis special processing, the resonant frequencies at observation points P_3–P_6 are relatively close to the reference value of 3.49 GHz [25], continuing to utilize Equation (19) (where E denotes the numerical results with and without the z-axis special processing, and E_{ref} corresponds to the value at 3.49 GHz), with an error of only about +0.28%. In contrast, the resonant frequency error without z-axis processing reaches approximately +6%, which has exceeded the range of small probability events (<5%). Finally, to verify the computational performance of the BOR-FDTD algorithm with and without z-axis special processing, Table 1 presents the comparison results of computational efficiency and memory consumption of the BOR-FDTD algorithm under Examples 1–3.

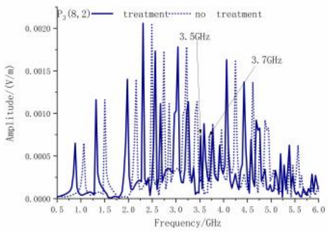

(a) Resonant frequency at observation Point P_3

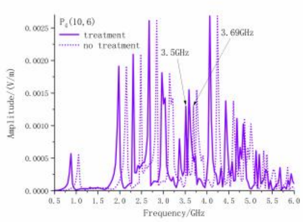

(b) Resonant frequency at observation Point P_4

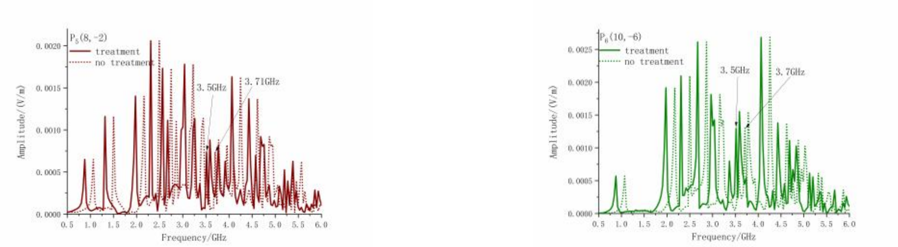

(c) Resonant frequency at observation Point P_5 (d) Resonant frequency at observation Point P_6

Fig. 10. The resonant frequencies at observation point P_3–P_6 in Example 3

Obviously, in the computational efficiency comparison, under Examples 1–3, the efficiency of the algorithm with *z*-axis special processing is lower than that without *z*-axis processing, but the reduction is only about 0.19%, 3.8%, and 2.9% respectively. In terms of memory comparison, the memory consumption with *z*-axis special processing is almost the same as that without *z*-axis processing (Example 1: 3%; Example 2: 1.3%; Example 3: 0.8%). Therefore, the on-axis processing method proposed in this paper has no significant impact on the computational efficiency and memory consumption of the BOR-FDTD algorithm (both are small probability events with a reduction or difference of less than 5%).

Table 1

The computational performance of BOR-FDTD with and without special treatment along the z-axis

		Example 1	Example 2	Example 3
Time(s)	With z-axis processing	252.4	2508.9	53.5
	Without z-axis processing	251.9	2412.4	51.9
Memory (Mb)	With z-axis processing	30.5	137.8	22.5
	Without z-axis processing	30.6	136	22.3

4. Conclusions

Since the evolution of the BOR-FDTD algorithm leverages axial symmetry to omit the angular differential discretization of FDTD and further reduces 3D spatial problems to a 2D plane, this evolutionary process introduces mathematical singularity in on-axis field quantities. Consequently, the lack of calculation for on-axis field quantities leads to computational errors. To address this issue, the main research work of this paper is as follows: Taking the differential discretization equations of BOR-FDTD as the starting point, the specific field quantities requiring on-axis special processing are identified through analysis. Using Stokes' theorem combined with the periodic cycle concept, the final equations for the 3D cylindrical FDTD field quantities (which need on-axis special processing) are derived by summing the electromagnetic field values at angular grid points. These equations are then converted to a 2D plane to obtain the final field quantities requiring special processing for the BOR-FDTD algorithm. The innovation of this study lies in proposing a numerical method to effectively handle the on-axis singularity problem.

Simulation results show that the on-axis special processing method for the BOR-FDTD algorithm can effectively improve computational accuracy without imposing an additional burden on computational efficiency. The significance of this research is mainly reflected in two aspects: On one hand, it fills the theoretical gap in the calculation of on-axis electromagnetic field quantities for the BOR-FDTD algorithm, solves the long-standing accuracy defect caused by on-axis singularity, and provides theoretical support for the precise application of this algorithm in electromagnetic simulation fields (such as optical fiber communication and microwave device design). On the other hand, the proposed processing idea of "derivation from 3D equations to 2D adaptation" also offers a reference paradigm for optimizing boundary/special point calculations in other FDTD-derived algorithms based on symmetry simplification.

However, this study still has certain limitations: The adaptability of the on-axis processing scheme under complex inhomogeneous medium models has not been fully verified. In addition, for ultra-large-scale electromagnetic simulation scenarios, further exploration is needed on how to optimize the calculation steps of equation solving to reduce memory consumption. Future research can focus on the following directions: Firstly, expand the example scenarios to verify the applicability of the scheme in inhomogeneous media and multi-scale models; Secondly, combine parallel computing technology to optimize the calculation process of on-axis equation solving, further enhancing the practicality of the algorithm in large-scale simulations.

REFERENCES

[1]. *H. Myo Tun*, "Development of Square Patch Microstrip Antenna Design by Using Three Dimension Finite Difference Time Domain Methods", JNEST, **vol. 2**, no. 3, 2023, pp. 83–88.

[2]. *K. Masumnia-Bisheh, C. Furse*, "Bioelectromagnetic Uncertainty Analysis Using Geometrically Stochastic FDFD Method", IEEE Transactions on Antennas and Propagation, **vol. 69**, no. 4, 2020, pp. 2433-2436.

[3]. *T. T. Koutserimpas, A. D. Papadopoulos, E. N. Glytsis*, "Applicability and Optimization of The Alternating Direction Implicit Iterative Method for the 2D Finite Difference Frequency Domain Solution of Scattering Problems", IEEE Transactions on Antennas and Propagation, **vol. 65**, no. 12, 2017, pp. 7166-7173.

[4]. *T. Jariyanorawiss, K. Kanjanasit, W. Chongburee, et al*, "SAR Analysis in an Anatomical Head Model Using CFL-Optimized Yee Cells and an Accurate Dipole Model at 700MHz for 5G Mobile Radiation", IEEE Access, **vol.13**, May. 2025, pp. 82718-82731.

[5]. *D.-Q. Vu, N.-N. Nguyen, T.-M. T. Le, et al*, "Computing Lightning-Induced Voltages on Overhead Distribution Lines Using the RBF-FDTD Approach", IEEE Access, **vol. 13**, July. 2025, pp. 125473–125484.

[6]. *T. Takagi, Y. Baba*, "FDTD Simulation of Electromagnetic Field, Heat, and Thermal Stress in a ZnO Element for Lightning Currents", IEEJ Transactions on Electrical and Electronic Engineering, **vol. 20**, no. 9, 2025, pp. 1470–1473.

[7]. *J. A. Pereda, A. Grande*, "On the Stability of the RK-FDTD Method for Graphene Modeling", IEEE Transactions on Antennas and Propagation, **vol. 73**, no. 10, 2025, pp. 8238–8241.

[8]. *A. Schroder, G. A. Rasek, H. D. Bruns, et al*, "Analysis of High Intensity Radiated Field Coupling into Aircraft Using the Method of Moments", IEEE Transactions on Electromagnetic Compatibility, **vol. 56**, no. 1, 2014, pp. 113-122.
[9]. *O. Ozgun, M. Kuzuoglu, R. Mittra*, "Self-Tuning Locally Conformal PML Mesh Truncation for 3D Vector Finite Element Method", IEEE Transactions on Antennas and Propagation, **vol. 72**, no. 2, 2024, pp. 2036-2040.
[10]. *G. Niu, W. J. Zhang, L. Xie, et al*, "Design and Optimization of a Corrugated Horn Feed with Axial and Radial Slots", Chinese Journal of Radio Science, **vol. 33**, no. 4, 2018, pp. 490-495.
[11]. *Y. Huangfu, L. Di Rienzo and S. Wang*, "FDTD Formulation Based on High-Order Surface Impedance Boundary Conditions for Frequency Dependent Lossy Multi-Conductor Transmission Lines", IEEE Transactions on Magnetics, **vol. 56**, no. 1, 2020, pp. 1-4.
[12]. *A. Firoozi, A. Mohammadi, R. Khordad, et al*, "Q-BOR-FDTD Method for Solving Schrodinger Equation for Rotationally Symmetric Nanostructures with Hydrogenic Impurity", Physica Scripta, **vol. 97**, no. 2, 2022, Art. no. 025802.
[13]. *Y. Zhang, Y. Kang, X. Feng, et al*, "Fast Analysis of Multi-Layered Anisotropic Electromagnetic Propagation Based on Z-transform Finite Difference Time Domain Method with Scale-Compressed Technique", Electromagn. Sci., **vol. 3**, no. 2, 2025, Art. no. 0100032.
[14]. *A. S. Pedgaonkar, J. J. Simpson, G. Moss*, "A Stochastic Scattered-Field FDTD Formulation Using a Highly Efficient FDTD Discrete Plane Wave Source for Weak Scattering Environments", IEEE Antennas and Wireless Propagation Letters, **vol. 24**, no. 8, 2025, pp. 2572–2576.
[15]. *G. Q. Dai, Z. H. Yu, L. Gao, et al*, "Research on Finite Difference Time Domain Method", Modern Electronics Technique, **vol. 36**, no. 1, 2013, pp. 140-143.
[16]. *D. W. Zhu, H. L. Chen, Z. W. Shen, et al*, "The Implementation of CPML/PML for Mixed-Order Fully Explicit BOR-FDTD Algorithm", Chinese Journal of Computational Physics, 2025, https://link.cnki.net/urlid/11.2011.O4.20250529.1950.007.
[17]. *S. Mirzaei-Ghormish, M. Shahabadi, D. Smalley*, "Body of Revolution Finite Difference Time Domain Modeling of Hybrid Plasmonic Ring Resonators", Opt. Express, **vol. 30**, 2022, pp. 36332-36342.
[18]. *L. J. Zhou, C. Wu, F. Yang, et al*, "Analysis of FZP Antenna System Based on HSG BOR FDTD", Chinese Institute of Electronics. Proceedings of 2013 National Annual Conference on Antennas (Upper Volume). School of Electronic Engineering, University of Electronic Science and Technology of China, 2013, pp. 560-563.
[19]. *J. H. Cui*, "Research on the Diffraction Characteristics of Symmetric Gratings in a Hollow Circular Dielectric Wave-guide", Qingdao University, 2021.
[20]. *T. Khemane, P. Padayachee, C. Shaw*, "Students 'Understanding of Stokes' Theorem in Vector Calculus", IEEE Transactions on Education, **vol. 67**, no. 4, 2024, pp. 550-561.
[21]. *S. Mirzaei-Ghormish, D. E. Smalley, M. Shahabadi, et al*, "Hybrid Dielectric Slot-Plasmonic Ring Resonator for Purcell Enhancement", Physica Scripta, **vol.** 98 no. 11, 2023, Art. no. 115030.
[22]. *R. Afzalsoltani, M. Davoodi, A. Pourdeilami*, "Numerical Site Response Modeling Using PML and Equivalent Linear Analysis: Validation with Field Data", Geotechnical and Geological Engineering, **vol.** 43, no. 7, 2025, Art. no. 366.
[23]. *K. Duru, B. Kalyanaraman, S. Wang*, "On the Stability Analysis of the Perfectly Matched Layer for the Elastic Wave Equation in Layered Media", Journal of Computational Physics, **vol. 540**, 2025, Art. no. 114268.
[24]. *W. S. Smith, A. Razmadze, X. M. Shao, et al*, "A Hierarchy of Explicit Low-Dispersion FDTD Methods for Electrically Large Problems", IEEE Transactions on Antennas and Propagation, **vol. 60**, no. 12, 2012, pp. 5787-5800.
[25]. *M. Taheri, D. Mirshekar-Syahkal*, "Accurate Determination of Modes in Dielectric-Loaded Cylindrical Cavities Using a One-Dimensional Finite Element Method", IEEE Transactions on Microwave Theory and Techniques, **vol. 37**, no. 10, 1989, pp. 1536-1541.